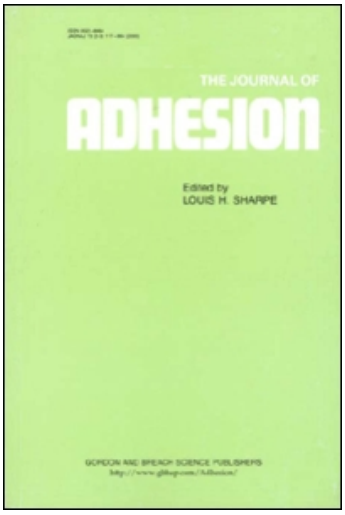

The Journal of Adhesion
Publication details, including instructions for authors and subscription information:
http://www.informaworld.com/smpp/title~content=t713453635

Analysis of the Tubular Single Lap Joint with Nonlinear Adhesive Properties

D. G. Lee[a]; K. S. Jeong[a]; J. H. Choi[a]
[a] Department of Precision Engineering and Mechatronics, Korea Advanced Institute of Science and Technology, Taejon-shi, Korea

To cite this Article Lee, D. G. , Jeong, K. S. and Choi, J. H.(1995) 'Analysis of the Tubular Single Lap Joint with Nonlinear Adhesive Properties', The Journal of Adhesion, 49: 1, 37 — 56
To link to this Article: DOI: 10.1080/00218469508009976
URL: http://dx.doi.org/10.1080/00218469508009976

J. Adhesion, 1995, Vol. 49, pp. 37–56
Reprints available directly from the publisher
Photocopying permitted by license only

Analysis of the Tubular Single Lap Joint with Nonlinear Adhesive Properties

D. G. LEE, K. S. JEONG and J. H. CHOI

Department of Precision Engineering and Mechatronics, Korea Advanced Institute of Science and Technology, Kusong-dong, Yusong-ku, Taejon-shi, Korea 305-701

(Received June 27, 1994; in final form October 11, 1994)

The majority of the load transfer of an adhesively-bonded joint is accomplished by the nonlinear behavior of the adhesive. In this paper, the torque transmission capability and shear stress distribution of the tubular single lap joint were calculated by incorporating the nonlinear shear properties of the adhesive. The nonlinear shear properties were represented by three different mathematical models such as two-parameter exponential, linear perfectly-plastic and multilinear strain-softening approximations.

From the analyses and experiments, it was found that all the analyses with nonlinear approximations predicted the torque transmission capabilities accurately, but the two-parameter exponential approximation gave the best predictions with the simplest form for use in numerical calculation.

KEY WORDS: adhesively-bonded tubular joint; nonlinear adhesive properties; strain softening; exponential approximation; elastic-plastic approximation; torque transmission capability.

INTRODUCTION

The design of joints has a special significance in fiber-reinforced composite structures because the joints are often the weakest areas in a composite structure and composite materials do not possess the forgiving characteristics of ductile metals, namely, their capacity to redistribute local high stresses by yielding.[1] For polymer matrix fiber reinforced composites, adhesive bonding and mechanical fasteners such as bolts and rivets can be utilized. Adhesive bonding is preferred for high performance continuous fiber reinforced polymer composite materials because of the continuous connection, whereas in drilling the holes for the bolts or rivets, fibers are cut, the joining is at discrete points, and large stress concentration occurs around each hole drilled.[2]

There are several types of adhesive joints, such as the single lap, the double lap, the stepped lap, and the scarf joint. Among these, the single lap joint has been studied more extensively than any other configuration through analytical, finite difference and finite element methods because the single lap joint is most popular, due to its ease of manufacture and its relatively low cost.

Several authors have studied the stresses in a tubular single lap joint subjected to torsion assuming elastic adhesive material properties. Alwar and Nagaraja used a finite element method to obtain the stresses in the tubular single lap joint subjected to torsion.[3] Adams and Peppiatt gave a closed form solution for the shear stresses in

tubular single lap joints and partially-tapered tubular scarf joints.[4] Graves and Adams used a finite element method to calculate the stresses of a tubular single lap joint whose adherends were orthotropic composite material subjected to torsion. They obtained the stresses in the adherends by the ply-by-ply analysis. Also, they obtained the stresses in the adherends with smeared laminate properties.[5]

Nonlinear adhesive property models have seen limited use in bondline analyses. Hart-Smith analyzed several adhesively-bonded joints such as the single lap, the double lap, the scarf, and the stepped lap joint. He chose an elastic-plastic model such that the total area under the stress-strain curve was equal to that under the true stress-strain curve and developed computer software for the analysis.[6] Grant modeled the adhesive stress-strain curve composed of elastic linear and plastic nonlinear curves.[7]

As mentioned before, many researchers have analyzed the stresses and the torque transmission capabilities of adhesively-bonded tubular lap joints and the related references are abundant. However, the previously-published calculation schemes could not predict accurately the torque transmission capability of the adhesively-bonded tubular lap joint when only the elastic properties of the adhesive were used. When the nonlinear adhesive properties were included, complicated mathematics was required for the analysis and much computing time was necessary,[8] even when a commercial finite element method was used, because the nonlinear shear properties of the adhesive could not be easily input to the material data module of the finite element method.

In this paper, the torque transmission capability and shear stress distribution of the tubular single lap joint were calculated by incorporating the nonlinear shear properties of the adhesive. The nonlinear shear properties were represented by three different curves such as the exponential approximation with two parameters, *i.e.*, the initial shear modulus and ultimate shear strength of the adhesive, the linear-elastic, perfectly-plastic approximation, and the multilinear, strain-softening approximation.

Using the nonlinear shear stress-strain curves, the torque transmission capability as well as the stress and strain distributions of the tubular single lap joint were calculated. Also, the validity of the analyses was checked experimentally by the measurement of the torque transmission capability of the tubular single lap joint.

ADHESIVE CONSTITUTIVE EQUATION

The shear stress-strain curves of adhesives are usually nonlinear. Figure 1(a) shows the shear stress-strain curves of a hot-cured, rubber-toughened epoxy adhesive[9] and Figure 1(b) shows the shear stress-strain curves of the FM-300 film adhesive at different temperatures.[10]

The majority of the load transfer of the adhesively-bonded joint is accomplished by the nonlinear behavior of the adhesive. The contribution of the linearly elastic behavior may be as little as 10% in the case of a ductile adhesive. Therefore, the torque transmission capability of the adhesively-bonded joint should be calculated taking into account the nonlinear behavior of the adhesive. The difficulty is how to characterize the adhesive.

In this paper, the shear stress, τ_a, *versus* shear strain, γ_a, curve of the adhesive was represented by the following three different curves.

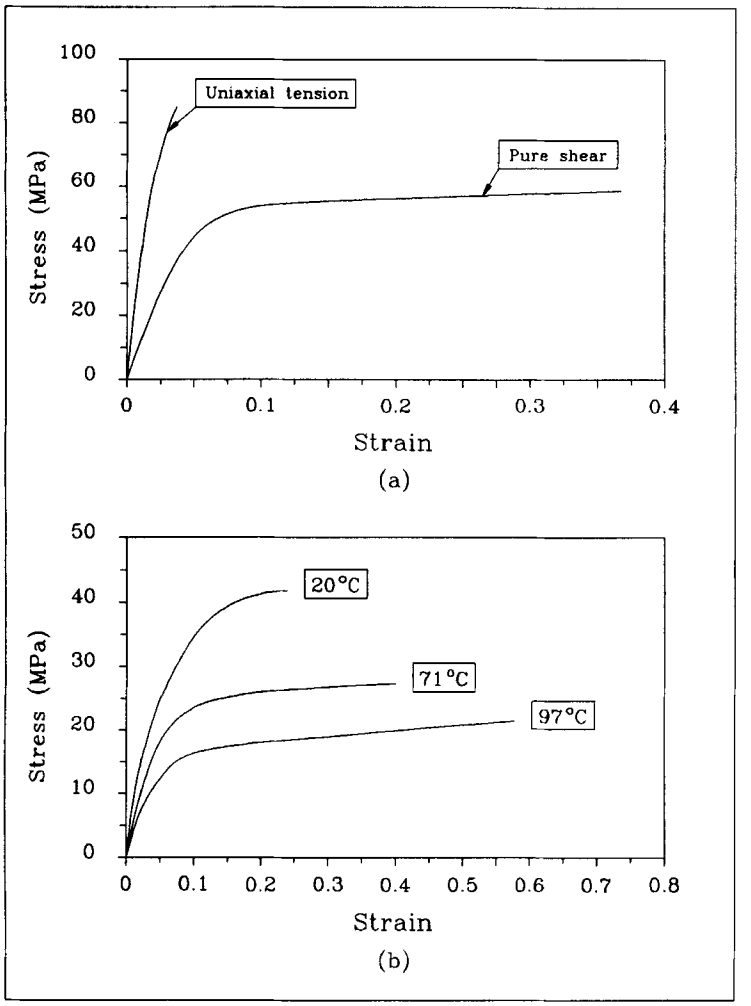

FIGURE 1 Shear stress-strain curves of the adhesives (a) Hot-cured, rubber-toughened epoxy adhesive (at 23°C), (b) FM-300 film adhesive.

The first shear stress-strain curve was represented using two parameters such as the initial shear modulus, G_a, and the ultimate shear strength, τ_m, as follows.

$$\tau_a = \tau_m \cdot (1 - e^{-Ga/\tau m \cdot \gamma a}) \tag{1}$$

where G_a and τ_m are functions of the environmental temperature. The two-parameter stress-strain curve can be determined if the two material properties, which can usually be obtained from the material suppliers, are known. The equation does not require the determination of the elastic limit of the shear strain. Figure 2(a) shows the shear stress-strain curve represented by the two-parameter exponential approximation and the experimentally-determined stress-strain curve for the IPCO 9923 epoxy adhesive whose material properties are shown in Table I.

TABLE I
Properties of IPCO 9923 epoxy adhesive

Tensile modulus (GPa)	1.30
Shear modulus (GPa)	0.46
Tensile strength (MPa)	39.5
Shear strength (MPa)	29.8
Shear strain limit (%)	23.5
Poisson's ratio	0.41
CTE (10^{-6} m/m °C)	72.0
Viscosity	Paste
Cure temperature (°C)	80.0
Cure time (minute)	270

Figure 2(b) shows the shear stress-strain curves represented by the two-parameter exponential approximation for the FM-300 film adhesive at different temperatures.

From Figure 2, the two-parameter exponential approximation was found to represent fairly well the shear stress-strain behavior of the adhesives.

The second shear stress-strain curve was represented using the linear-elastic, perfectly-plastic curve as follows.

$$\begin{aligned} \tau_a &= G_a \cdot \gamma_a \quad (\gamma_a \leq \gamma_y) \\ &= \tau_m \quad (\gamma_a > \gamma_y) \end{aligned} \tag{2}$$

where τ_m and γ_y are the ultimate shear stress and the yielding shear strain of the adhesive.

Figure 3 shows the shear stress-strain curve represented by the linear-elastic, perfectly-plastic approximation.

The third shear stress-strain curve was represented using the multilinear elastic strain-softening curve as follows.

$$\begin{aligned} \Delta\tau_a &= G_i \cdot \Delta\gamma_i \quad (\gamma_i < \gamma_a < \gamma_{i+1}) \\ \tau_a &= \sum_{i=0}^{n} G_i \cdot \Delta\gamma_i \quad (i = 0, 1, 2, \ldots, n) \end{aligned} \tag{3}$$

Figure 4 shows the shear stress-strain curve represented by the multilinear elastic strain-softening approximation. In this paper, five elastic strain-softening regions were used.

ANALYSIS OF THE TUBULAR SINGLE LAP JOINT

In order to derive the governing equation for the shear strain distribution, several assumptions were made: the adherends were made of elastic materials, the adhesive and the adherends were under only shear stresses. The governing equations derived with these assumptions can be applied also to the joint whose adherends are made of

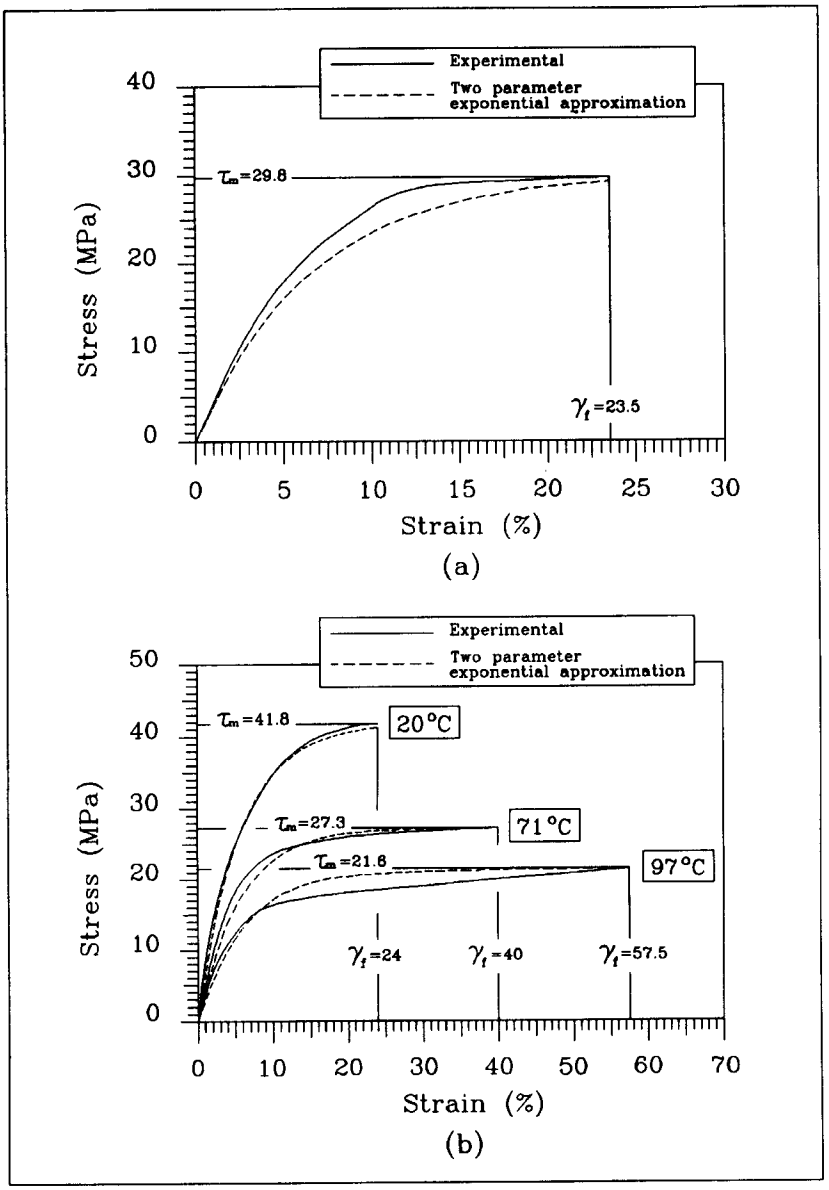

FIGURE 2 Shear stress-strain curve represented by the two-parameter exponential approximation and the experimentally-determined curve: (a) IPCO 9923 epoxy adhesive (at 25°C), (b) FM-300 film adhesive (at 20 °C; G_a = 0.74 GPa, at 71 °C; G_a = 0.48 GPa and at 91 °C; G_a = 0.35 GPa).

orthotropic composite materials. Figure 5 shows the geometric shape and nomenclatures of the tubular single lap joint for analysis.

From the torque equilibrium, the sum of the torques T_1 and T_2 in the inner and outer adherends of Figure 5 should be equal to the applied torque, T, that is, the following

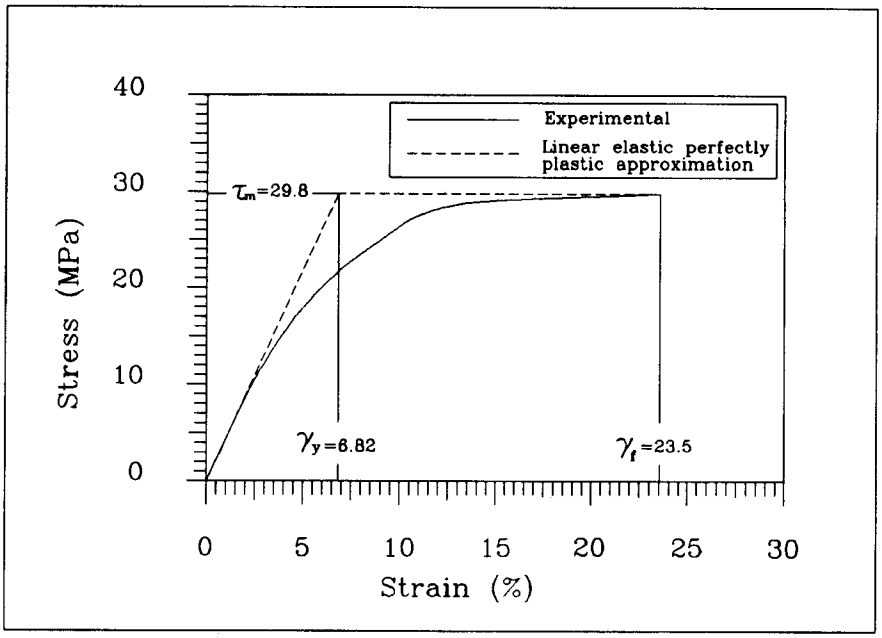

FIGURE 3 Shear stress-strain curve represented by the linear-elastic, perfectly-plastic approximation and the experimentally-determined curve for the IPCO 9923 adhesive.

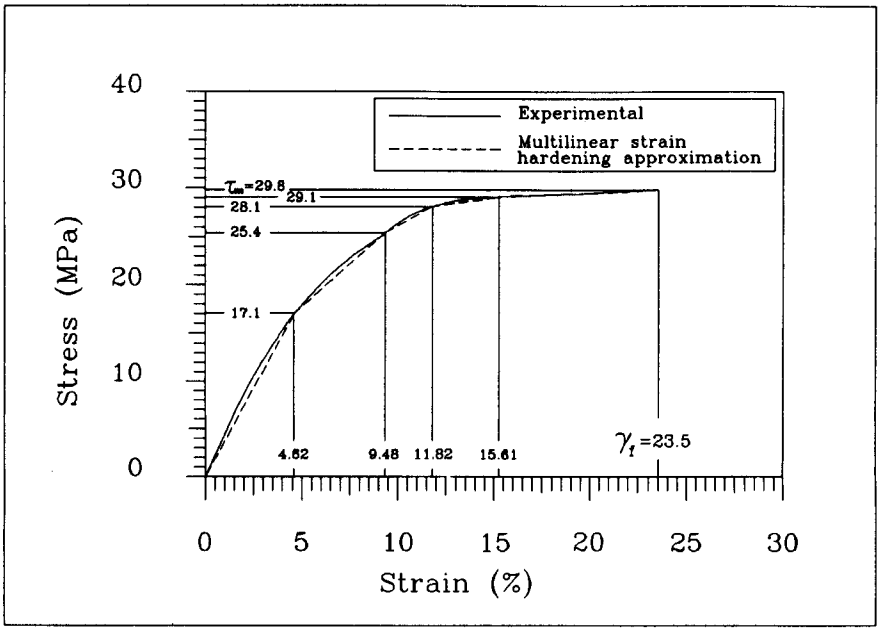

FIGURE 4 Shear stress-strain curve represented by the multilinear strain hardening approximation and the experimentally-determined curve for the IPCO 9923 adhesive.

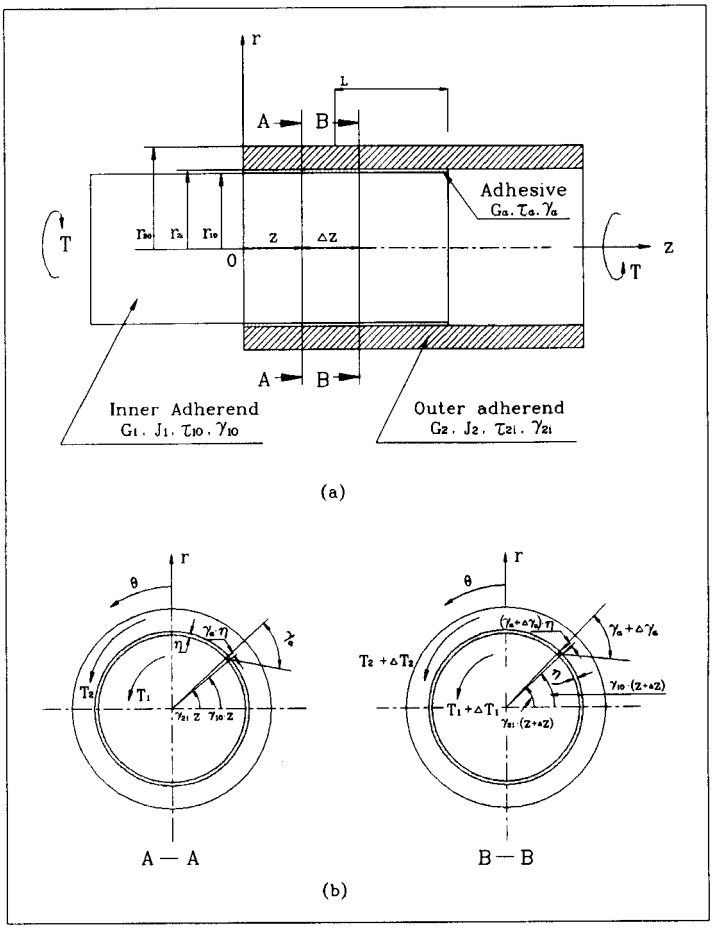

FIGURE 5 Geometric shape of the adhesively-bonded tubular single lap joint: (a) Shape of the single lap joint (b) Cross sections of the joint.

equation should hold through the adhesive length

$$T = T_1 + T_2 = \frac{\tau_{1o} \cdot J_1}{r_{1o}} + \frac{\tau_{2i} \cdot J_2}{r_{2i}} = \text{constant} \tag{4}$$

where τ_{1o} is the shear stress of the inner adherend at radius r_{1o}, τ_{2i} the shear stress of the outer adherend at radius r_{2i}, J_1 the sectional polar moment of inertia of the inner adherend, and J_2 the sectional polar moment of inertia of the outer adherend.

Assuming small adhesive thickness, η, and considering an element of the joint length, Δz, as shown in Figure 5b, geometric compatibility yields the following relationship.

$$\eta(\gamma_a + \Delta\gamma_a) - \eta \cdot \gamma_a = \gamma_{2i} \cdot \Delta z - \gamma_{1o} \cdot \Delta z \tag{5}$$

where, γ_{1o} is the shear strain of the inner adherend at r_{1o}, and γ_{2i} is the strain of the outer adherend at r_{2i}.

In the limit that Δz becomes infinitesimally small, Eq. (5) reduces as follows.

$$\eta \cdot \frac{d\gamma_a}{dz} = \gamma_{2i} - \gamma_{1o} \tag{6}$$

Assuming that the adhesive is an isotropic material and that the thickness of the adhesive is small, the variations of the torque in the z-direction are expressed as follows.

$$\frac{dT_1}{dz} = -2\pi \cdot a^2 \cdot \tau_a \tag{7}$$

$$\frac{dT_2}{dz} = 2\pi \cdot a^2 \cdot \tau_a \tag{8}$$

where, $a(=r_{1o}+r_{2i}/2)$ is the average radius of the adhesive.

Using the geometric compatibility and torque equilibrium equations so far derived, the governing equation of the adhesive can be calculated according to the three adhesive constitutive relationships:

(1) Two Parameter Exponential Approximation

The geometric compatibility between the shear strain of the adhesive and the shear strains of the adherends can be written as follows.

$$\begin{aligned} \frac{d\gamma_a}{dz} &= \frac{\gamma_{2i} - \gamma_{1o}}{\eta} = \frac{1}{\eta}\left(\frac{T_2 \cdot r_{2i}}{G_2 \cdot J_2} - \frac{T_1 \cdot r_{1o}}{G_1 \cdot J_1}\right) \\ &= \frac{1}{\eta}\left\{\frac{T \cdot r_{2i}}{G_2 \cdot J_2} - \left(\frac{r_{1o}}{G_1 \cdot J_1} + \frac{r_{2i}}{G_2 \cdot J_2}\right) \cdot T_1\right\} \end{aligned} \tag{9}$$

where, G_1 and G_2 are the shear moduli of the inner and outer adherend, respectively. Differentiating Eq. (9) with respect to z, the following equation can be obtained.

$$\frac{d^2\gamma_a}{dz^2} = -\frac{1}{\eta}\left(\frac{r_{1o}}{G_1 \cdot J_1} + \frac{r_{2i}}{G_2 \cdot J_2}\right) \cdot \frac{dT_1}{dz} \tag{10}$$

Substituting Eq. (1) into Eq. (7) and then substituting the resulting equation into Eq. (10) results in the governing differential equation of the shear strain of the adhesive as follows.

$$\begin{aligned} \frac{d^2\gamma_a}{dz^2} &= \frac{2\pi \cdot a^2}{\eta} \cdot \left(\frac{r_{1o}}{G_1 \cdot J_1} + \frac{r_{2i}}{G_2 \cdot J_2}\right) \cdot \tau_m \cdot (1 - e^{-(G_a/\tau_m)\cdot\gamma_a}) \\ &= \mu \cdot \tau_m \cdot (1 - e^{-(G_a/\tau_m)\cdot\gamma_a}) \end{aligned} \tag{11}$$

where

$$\mu = \frac{2\pi \cdot a^2}{\eta} \cdot \left(\frac{r_{1o}}{G_1 \cdot J_1} + \frac{r_{2i}}{G_2 \cdot J_2}\right) \tag{12}$$

Since $T_1 = T$, $T_2 = 0$, when $z = 0$, the following boundary conditions are obtained from Eq. (6) and Eq. (11).

$$\left.\frac{d\gamma_a}{dz}\right]_{z=0} = \gamma_a'(0) = -\frac{1}{\eta}\cdot\left(\frac{T\cdot r_{1o}}{G_1\cdot J_1}\right) \tag{13}$$

$$\left.\frac{d^2\gamma_a}{dz^2}\right]_{z=0} = \gamma_a''(0) = \mu\cdot\tau_m\cdot(1 - e^{-(G_a/\tau_m)\cdot\gamma_a(0)}) \tag{14}$$

Differentiating Eq. (14), the third order derivative boundary condition is obtained as follows.

$$\left.\frac{d^3\gamma_a}{dz^3}\right]_{z=0} = \gamma_a'''(0) = \mu\cdot G_a\cdot(e^{-(G_a\tau_m)\cdot\gamma_a(0)})\cdot\gamma_a'(0) \tag{15}$$

Since $T_1 = 0$, $T_2 = T$ when $z = L$, another boundary condition is obtained as follows.

$$\left.\frac{d\gamma_a}{dz}\right]_{z=L} = \gamma_a'(L) = \frac{1}{\eta}\cdot\left(\frac{T\cdot r_{2i}}{G_2\cdot J_2}\right) \tag{16}$$

Equation (11) was solved by a numerical method using the Taylor series expansion method[11] including maximum third order derivative as follows.

$$\gamma_a(z+h) = \gamma_a(z) + \gamma_a'(z)\cdot h + \gamma_a''(z)\cdot\frac{h^2}{2} + \gamma_a'''(z)\cdot\frac{h^3}{6} + \cdots \tag{17}$$

$$\gamma_a'(z+h) = \gamma_a'(z) + \gamma_a''(z)\cdot h + \gamma_a'''(z)\cdot\frac{h^2}{2} + \cdots \tag{18}$$

$$\gamma_a''(z+h) = \gamma_a''(z) + \gamma_a'''(z)\cdot h + \cdots \tag{19}$$

$$\gamma_a'''(z+h) = \gamma_a'''(z) + \cdots \tag{20}$$

where $\gamma_a(z)$ is the shear strain at distance z and h is the incremental distance along the z-axis.

The maximum torque transmission capability was calculated by assuming that either one or the other end of the adhesive reached the failure shear strain γ_f. Since the magnitude of the first derivative of the shear strain, γ_a', becomes smaller as the shear strain approaches the failure strain, the end which reaches the failure strain first was determined by comparing $|\gamma_a'(0)|$ and $|\gamma_a'(L)|$. Then the other end should satisfy the condition of the first derivative of the shear strain. Since the first derivative contains the applied torque, T, this condition gives the maximum torque. In this paper, the first adhesive failure occurred at $z = 0$. In the numerical calculation, the first trial value of T was calculated by assuming that all the adhesive area reaches the ultimate shear stress, τ_m, and then the value of torque was decreased successively to satisfy the first derivative of the boundary conditions.

(2) Linear-Elastic-Perfectly-Plastic Approximation

In Figure 6, it is assumed that the regions I and III reach the perfectly-plastic zone whose shear stress is constant, τ_m, and region II is in the elastic zone. Two sections $z = L_{Y1}$ and $z = L - L_{Y2}$ are the boundaries of the elastic and plastic zones.

The analysis was performed in three different regions.

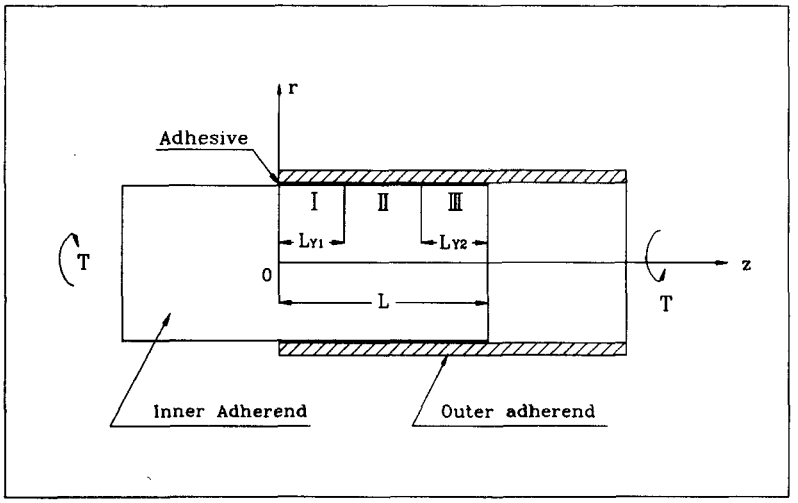

FIGURE 6 Linear elastic and perfectly plastic zones in the bonding length.

⟨Region I⟩

Since the adhesive shear stress was assumed to be the constant, τ_m, in region $I(0 < z < L_{Y1})$ of the adhesive, the variation of torque with respect to z in the region I can be expressed as follows:

$$\frac{dT_2}{dz} = 2\pi a^2 \cdot \tau_m = -\frac{dT_1}{dz} \tag{21}$$

The boundary condition of Eq. (21) at $z = 0$ is as follows.

$$\text{When } z = 0, \quad T_2 = \tau_{2i} = 0 \tag{22}$$

Integrating Eq. (21) and using the boundary condition of Eq. (22), the torques T_1 and T_2 can be calculated as follows:

$$T_1 = T - 2\pi a^2 \cdot \tau_m \cdot z = \frac{\tau_{1o} \cdot J_1}{r_{1o}} \tag{23}$$

$$T_2 = 2\pi a^2 \cdot \tau_m \cdot z = \frac{\tau_{2i} \cdot J_2}{r_{2i}} \tag{24}$$

The geometric compatibility Eq. (9) becomes the following:

$$\frac{d\gamma_a}{dz} = \frac{1}{\eta}(2A \cdot z - B) \tag{25}$$

Where,

$$A = \left(\frac{r_{1o}}{G_1 \cdot J_1} + \frac{r_{2i}}{G_2 \cdot J_2}\right)\pi a^2 \cdot \tau_m \tag{26}$$

$$B = \frac{r_{1o}}{G_1 \cdot J_1} T \tag{27}$$

The boundary condition of Eq. (25) is:

When

$$z = L_{Y1}, \quad \gamma_a = \gamma_y = \frac{\tau_m}{G_a} \tag{28}$$

Integrating Eq. (25) with the boundary conditions of Eq. (28), the shear strain of the adhesive can be calculated as follows:

$$\gamma_a = \frac{\tau_m}{G_a} + \frac{1}{\eta}[A(z^2 - L_{Y1}^2) - B(z - L_{Y1})] \tag{29}$$

⟨Region II⟩

Since region II($L_{Y1} < z < L - L_{Y2}$) of the adhesive was assumed to be an elastic zone, the variation of the torque with respect to z was expressed in Eq. (7) and (8) as follows:

$$\frac{dT_2}{dz} = 2\pi a^2 \cdot \tau_a = -\frac{dT_1}{dz} \tag{30}$$

Differentiating Eq. (30) with the geometric compatibility of Eq. (6) yields the following equation.

$$\frac{d^2T_2}{dz^2} = 2\pi a^2 \cdot \frac{G_a}{\eta} \cdot (\gamma_{2i} - \gamma_{1o}) \tag{31}$$

Substituting T_2 of Eq. (4) into Eq. (31), the following shear stress equation is derived:

$$\frac{d^2\tau_{2i}}{dz^2} - \alpha^2 \tau_{2i} = -\delta \frac{T \cdot r_{2i}}{J_2} \tag{32}$$

where δ, ϕ, α are defined below.

$$\delta = \frac{2\pi \cdot a^2 \cdot r_{1o} \cdot G_a}{G_1 \cdot J_1 \cdot \eta} \tag{33}$$

$$\phi = \frac{G_2 \cdot J_2 \cdot r_{1o}}{G_1 \cdot J_1 \cdot r_{2i} + G_2 \cdot J_2 \cdot r_{1o}} \tag{34}$$

$$\alpha = \left(\frac{\delta}{\phi}\right)^{0.5} \tag{35}$$

From Eq. 24, the boundary conditions of Eq. (32) are:
When $z = L_{Y1}$,

$$\tau_{2i} = \frac{2\pi a^2 \cdot r_{2i} \cdot \tau_m}{J_2} \cdot L_{Y1} = D \tag{36}$$

When $z = L - L_{Y2}$,

$$\tau_{2i} = \frac{T \cdot r_{2i}}{J_2} - \frac{2\pi a^2 \cdot r_{2i} \cdot \tau_m}{J_2} \cdot L_{Y2} = E \tag{37}$$

Using the boundary conditions of Eqs. (36) and (37) and integrating Eq. (32), τ_{2i} is obtained as follows:

$$\tau_{2i} = C_1 \cdot \cosh(\alpha z) + C_2 \cdot \sinh(\alpha z) + \phi \frac{r_{2i}}{J_2} T \tag{38}$$

where C_1 and C_2 are as defined below.

$$C_1 = \frac{1}{F}\left[\sinh(\alpha(L - L_{Y2})) \cdot \left(D - \phi \frac{r_{2i}}{J_2} T\right) - \sinh(\alpha L_{Y1}) \cdot \left(E - \phi \frac{r_{2i}}{J_2} T\right)\right] \tag{39}$$

$$C_2 = \frac{1}{F}\left[\cosh(\alpha L_{Y1}) \cdot \left(E - \phi \frac{r_{2i}}{J_2} T\right) - \cosh\left(\alpha \cdot (L - L_{Y2}) \cdot D - \phi \frac{r_{2i}}{J_2} T\right)\right] \tag{40}$$

Also, F is defined as follows.

$$F = \cosh(\alpha L_{Y1}) \cdot \sinh(\alpha \cdot (L - L_{Y2})) - \sinh(\alpha L_{Y1}) \cdot \cosh(\alpha \cdot (L - L_{Y2})) \tag{41}$$

Since T_2 can be calculated from Eq. (38), the shear stress, τ_a, of the adhesive can be calculated by substituting dT_2/dz into Eq. (30):

$$\tau_a = \frac{J_2}{2\pi a^2 \cdot r_{2i}} [C_1 \alpha \cdot \sinh(\alpha z) + C_2 \alpha \cdot \cosh(\alpha z)] \tag{42}$$

⟨Region III⟩

In region III ($L - L_{Y2} < z < L$) of the adhesive, the variation of the torque with respect to z is:

$$\frac{dT_2}{dz} = 2\pi a^2 \cdot \tau_m = -\frac{dT_1}{dz} \tag{43}$$

The boundary conditions of Eq. (43) are:
When $z = L$,

$$\tau_{2i} = \frac{T \cdot r_{2i}}{J_2} \tag{44}$$

And, when $z = L - L_{Y2}$,

$$\gamma_y = \frac{\tau_m}{G_a} \tag{45}$$

Using the boundary conditions of Eqs. (44) and (45), the strain, γ_a, of the adhesive in region III can be calculated by the same method as in region I:

$$\gamma_a = \frac{\tau_m}{G_a} - \frac{1}{\eta}[A\cdot(z^2 - 2Lz + L^2 - L_{Y2}^2) + B'(z - L + L_{Y2})] \tag{46}$$

where B' is defined is as:

$$B' = \frac{r_{2o}}{G_2 \cdot J_2} T \tag{47}$$

Since the adhesive shear stress, τ_a, in Eq. (42) is τ_m at both $z = L_{Y1}$ and $z = L - L_{Y2}$, two relationships between L_{Y1}, L_{Y2} and T can be obtained. If the value of L_{Y1} (or L_{Y2}) is given, the value of L_{Y2} (or L_{Y1}) and T can be numerically calculated from the two relationships. Then, using Eq. (29) and Eq. (46), the shear strains at $z = 0$ and $z = L$ can be calculated. If the shear strain at either end of the joint does not reach the failure shear strain of the adhesive, the value of L_{Y1} (or L_{Y2}) is increased and the previous steps are repeated until the shear strain at either end of the joint reaches the failure shear strain of the adhesive. The value of T becomes the torque transmission capability of the adhesively-bonded joint when the shear strain at either end reaches the failure shear strain of the adhesive. Also, the distribution of the shear stress, τ_a, in region II is obtained by Eq. (42) and the distributions of the shear strains in regions I and III are obtained by Eq. (29) and (46), respectively. Since the maximum shear strain of the adhesive occurs at either one or other end of the adhesive, the two shear strains at the ends of the adhesive were calculated and compared.

(3) Multilinear Strain-Softening Approximation

It is very hard to get the closed form solution of the adhesive joint with the linear strain softening approximation as shown in Figure 4. Therefore, the finite element method was used in the analysis of the adhesively-bonded tubular single lap joint with the linear strain-softening adhesive properties. The finite element programm used was ANSYS 5.0[12] in which and 8-Node 3-D isoparametric element was used for the analysis. Since the tubular joint has geometric symmetry, a quarter of the whole structure was analyzed. Figure 7 represents the element of the cross-section of the tubular single lap joint.

Also, the closed form solution for the torque transmission capabilities of the adhesively-bonded tubular single lap joint with linear elastic shear properties of the adhesive, which was derived by Adams,[4] is included in the Appendix of this paper.

NUMERICAL COMPUTATIONS AND EXPERIMENTS

In order to verify the validity of the method developed in this work, the tubular single lap joints were tested under static torque. Figure 8 and Table II show the dimensions and data for the adhesively-bonded single lap joint used in computations and experiments.

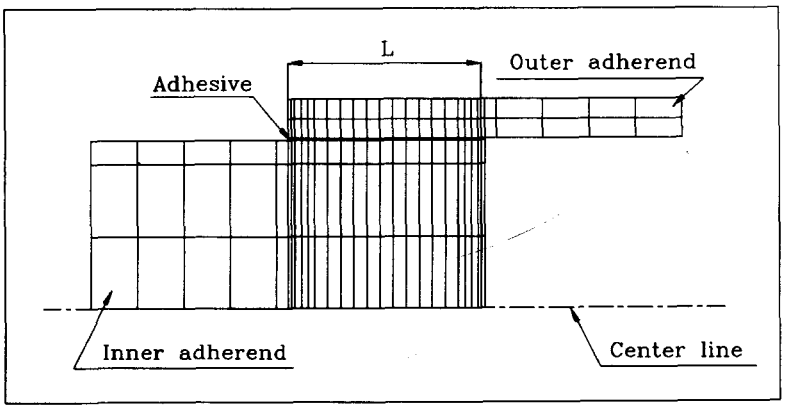

FIGURE 7 Finite element mesh model of the tubular single lap joint.

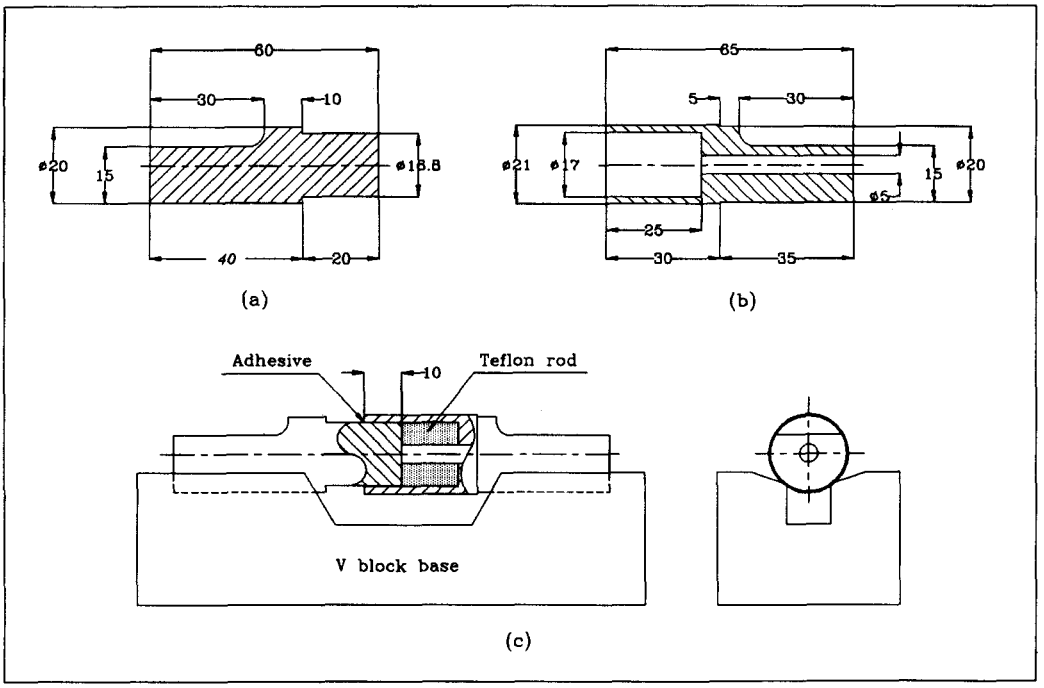

FIGURE 8 Dimensions(mm) of the adherends of the tubular single lap joint: (a) Inner adherend (b) Outer adherend (c) Assembled tubular single lap joint.

Figure 9 shows the shear stress and strain distributions in the adhesive of the single lap joint when the bonding length is 10 mm and the applied torque is 120 N·m. From Figure 9, it was found that the shear stresses calculated by the three constitutive relations were not much different, while the shear strains were much different because

TABLE II
Data of the adhesively-bonded tubular single lap joint

	Adhesive (IPCO 9923)	Inner adherend (Steel solid rod)	Outer adherend (Steel hollow tube)
Shear modulus (GPa)	0.46	80.0	80.0
Sectional polar moment of inertia (10^{-9} m^4)	–	7.82	10.89
Thickness (mm)	0.1	–	2.0
Inner radius (mm)	8.4	–	8.5
Outer radius (mm)	8.5	8.4	10.5
Bonding length (mm)		10	

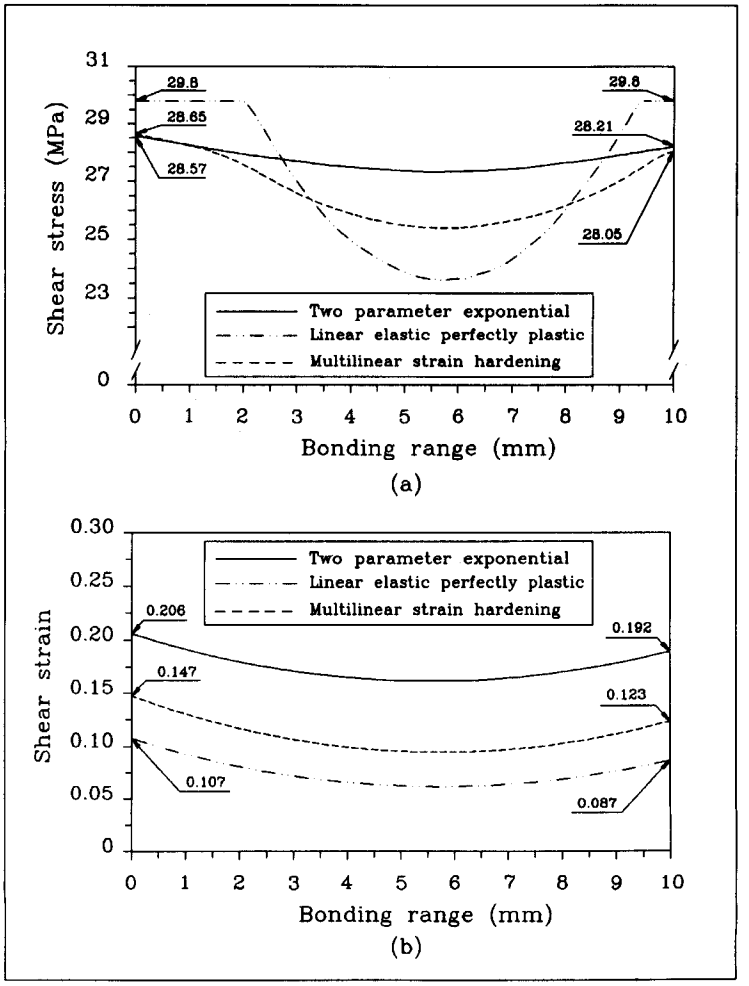

FIGURE 9 Shear stress and strain distributions in the adhesive when the bonding length is 10 mm and the applied torque is 120 N.m.: (a) Shear stress distributions (b) Shear strain distributions.

the majority of the adhesive was under a shear stress close to the ultimate shear strength due to the shear-strain-softening effect. If the ultimate shear strain of the adhesive was small or if the shear-softening effect was small, the approximation model that was fitted well to the physical behavior would accurately predict the shear stress distribution. The shear strains at the two ends of the joint are different because the joint is not symmetric to the plane which is perpendicular to the z-axis, which is evident from the elastic closed-form solution in the Appendix of the paper.

Figure 10 and 11 show the shear stress and strain distributions, respectively, in the adhesive, when the joint whose bonding length is 10 mm, reaches the value of the failure shear strain, 0.235.

In order to check the validity of the analyses, several adhesively-bonded tubular single lap joints were manufactured and tested. Since the torque transmission capability of the adhesively-bonded tubular single lap joint depends on the surface roughness of the adherends and the thickness of adhesive, in this paper an arithmetric surface roughness of 2 μm of the adherends and a thickness of adhesive of 0.1 mm were chosen, because these values were suggested to be the optimum for the fatigue strength of the same testpiece.[13] Both the inner and outer adherends have accurate mounting surfaces which were ground, and the concentricity between the outer and inner adherends was secured by mounting the ground surfaces in an accurate V-block when curing the adhesive. Ten joint specimens were manufactured and tested under static torque with the multiaxial material testing system MTS 319.10.[14]

Table III shows the maximum torque transmission capabilities which were experimentally measured and calculated using the three different nonlinear approximations. From Table IV, it was found that all three nonlinear approximations accurately predicted the torque transmission capabilities with an error of less than 5%. The two-parameter exponential approximation method slightly underestimated while the other two methods overestimated the experimentally-determined torque transmission capability. Since the two-parameter capability exponential approximation method not only gives better prediction but also has the simpler form to be used in the numerical calculation, it is recommended for the analysis and design of adhesively-bonded tubular single lap joints.

CONCLUSIONS

In this work, the shear strain and shear stress distributions and torque transmission capabilities of the tubular single lap joint were calculated by incorporating nonlinear adhesive shear stress-strain properties. The nonlinear shear properties of the adhesive were represented by three different approximation methods: two-parameter exponential, linear-elastic perfectly-plastic and multilinear strain-softening approximations. In order to check the validity of the analyses, the torque transmission capabilities of the tubular single lap joints were experimentally tested.

From the tests, it was found that all of the nonlinear approximations accurately predicted the torque transmission capabilities of the tubular single lap joint. The two-parameter exponential approximation best predicted the torque transmission capabilities and it has the simplest form for use in the numerical calculation.

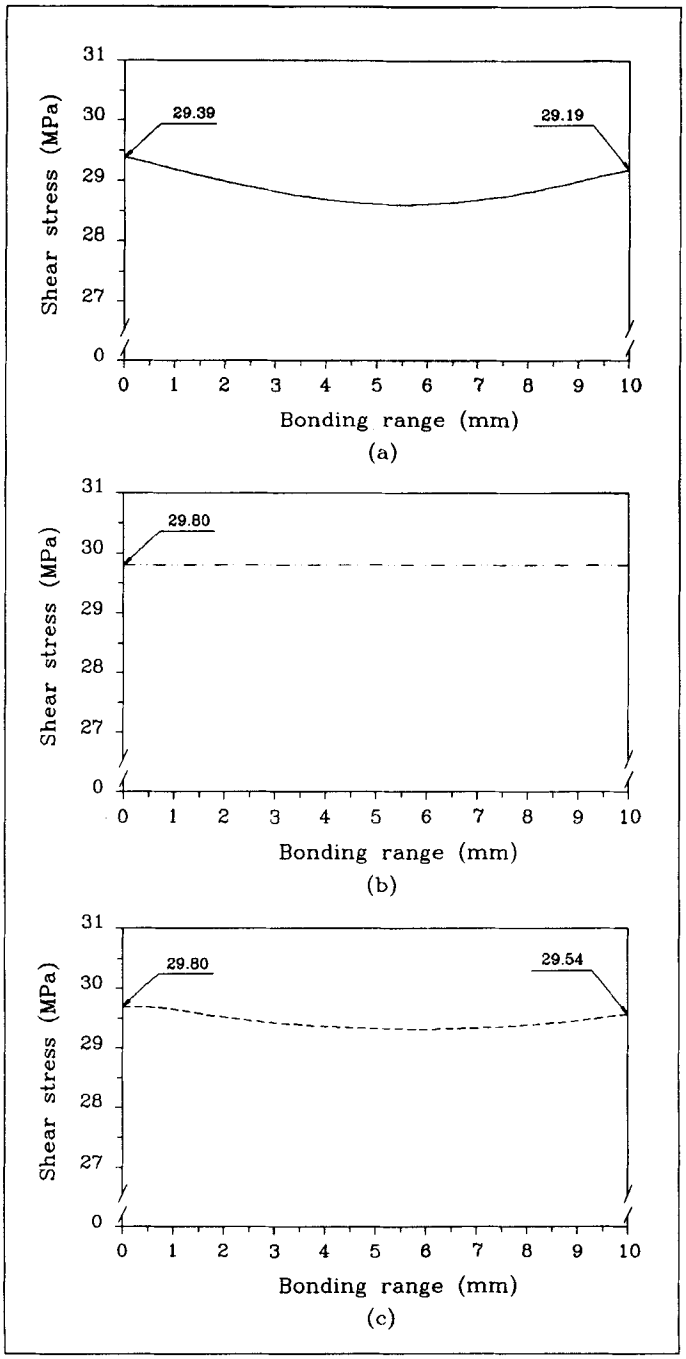

FIGURE 10 Shear stress distributions in the adhesive when the adhesive maximum shear strain reaches the adhesive failure strain, 0.235 (adhesive bonding length: 10 mm): (a) Two-parameter exponential approximation, (b) Linear-elastic, perfectly-plastic approximation, (c) Multilinear strain hardening approximation.

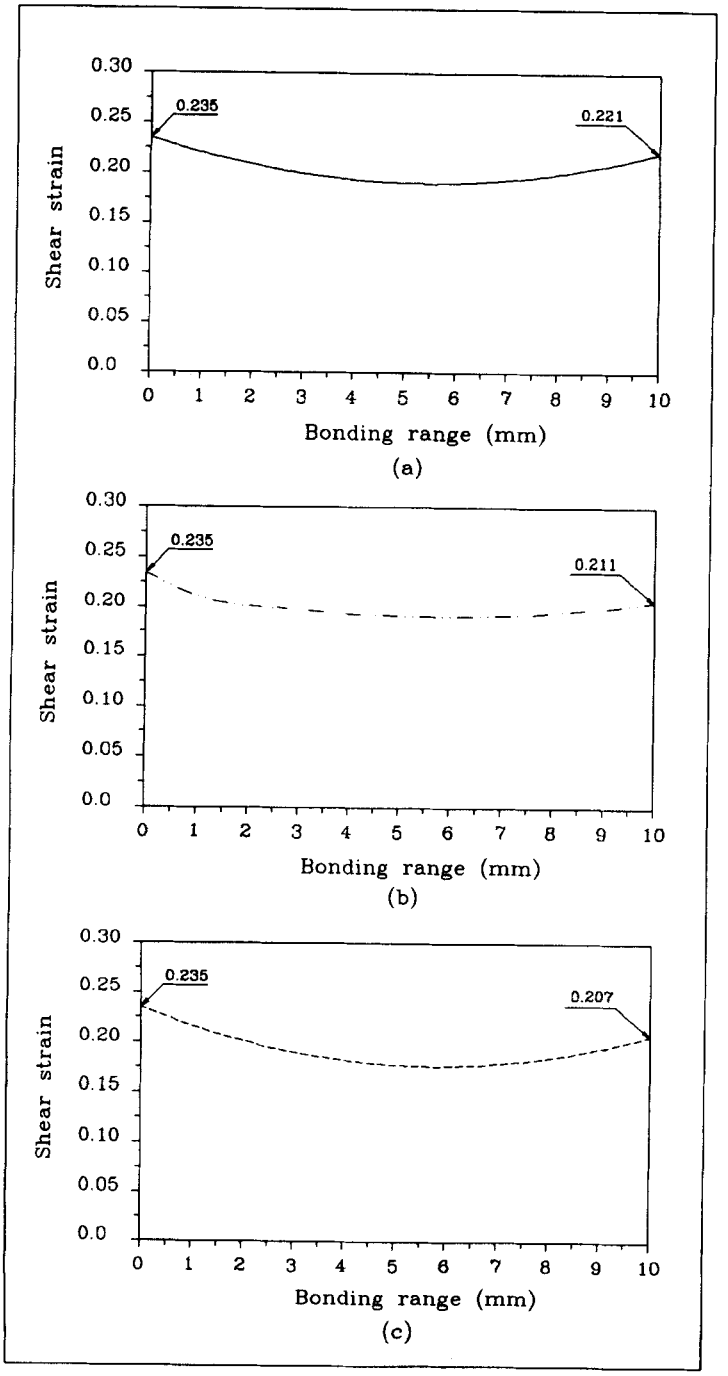

FIGURE 11 Shear strain distributions in the adhesive when the adhesive maximum shear strain reaches the adhesive failure strain, 0.235 (adhesive bonding length: 10 mm): (a) Two-parameter exponential approximation, (b) Linear-elastic, perfectly-plastic approximation, (c) Multilinear strain hardening approximation.

TABLE III
Maximum torque transmission capabilities of the tubular single lap joints

Experiment	Maximum torque (N·m) Average 128.1 Standard deviation 2.6	Error
Two-parameter exponential approximation	127.6	−0.4(%)
Linear elastic perfectly plastic approximation	133.4	+4.1(%)
Multilinear strain softening approximation	131.8	+2.9(%)

References

1. P. K. Mallick, *Fiber-Reinforced Composites* (Marcel Dekker, Inc., New York and Basel, 1988), Chap. 6.
2. J. R. Vinson and R. L. Sierakowski, *The Behavior of Structures Composed of Composite Materials* (Martinus Nijhoff Publishers, 1987), Chap. 8.
3. R. S. Alwar and Y. R. Nagaraja, "Viscoelastic Analysis of an Adhesive Tubular Joint," *J. Adhesion* **8**, 79–92 (1976).
4. R. D. Adams and N. A. Peppiatt, "Stress Analysis of Adhesive Bonded Tubular Lap Joints," *J. Adhesion* **9**, 1–18 (1977).
5. S. R. Graves and D. F. Adams, "Analysis of a Bonded Joint in a Composite Tube Subjected to Torsion," *J. Composite Materials* **15**, 211–224 (1981).
6. L. J. Hart-Smith, "Further Developments in the Design and Analysis of Adhesive Bonded Structural Joints," in *Joining of Composite Materials*, ASTM STP **749**, 3–31 (1981).
7. P. Grant, "Analysis of Adhesive Stresses in Bonded Joints," *Symposium: Jointing in Fibre Reinforced Plastics*, (IPC Science and Technology Press, Imperial College, London, Guildford, UK 1978), p. 41.
8. R. D. Adams, "Theoretical Stress Analysis of Adhesively Bonded Joints," in *Joining Fiber-reinforced Plastics*, F. L. Matthews, Ed. (Elsevier Applied Science, London and New York, 1986), pp. 185–226.
9. T. A. Osswald and J. Rietveld, "Measuring Constitutive Properties," in *Adhesives and Sealants* (ASM International, Metals Park, Ohio, 1990), p. 315.
10. A. A. Baker, "Repair Techniques for Composite Structures," in *Composite Materials in Aircraft Structures*, D. H. Middleton, Ed. (Longman Scientific & Technical, New York, 1990), p. 215.
11. F. B. Hildebrand, *Advanced Calculus for Applications*, 2nd ed. (Prentice-Hall, Inc., New Jersey, 1976), Chap. 3.
12. *ANSYS User's Manual* (Swanson Analysis Systems, Inc., Houston, U.S.A., 1992).
13. D. G. Lee, K. S. Kim and Y. T. Lim, "An Experimental Study of Fatigue Strength for Adhesively Bonded Tubular Single Lap Joints," *J. Adhesion* **35**, 39–53 (1991).
14. MTS Instruments, Minneapolis, Minnesota, U.S.A.

APPENDIX

Assuming that the adhesive is a linear material, stress and strain distributions of the tubular single lap joint of Figure 5 were calculated as follows:[4]

Differentiating Eq. (8) w.r.t. z, and using the relationships $T_2 = \tau_{2i} J_2 / r_{2i}$, $\gamma_{2i} = \tau_{2i}/G_2$ and $\gamma_{1o} = \tau_{1o}/G_1$, the following equation involving τ_{2i} is obtained

$$\frac{d^2\tau_{2i}}{dz^2} = 2\pi a^2 \frac{r_{2i} G_a}{J_2 \eta}\left(\frac{\tau_{2i}}{G_2} - \frac{\tau_{1o}}{G_1}\right). \tag{48}$$

Substituting τ_{1o} from Eq. (4) into Eq. (48) and noting that at $z = L$, $T = (\tau_{2iL} J_2 / r_{2i})$, Eq. (48) becomes the following equation

$$\frac{d^2\tau_{2i}}{dz^2} = 2\pi a^2 \frac{G_a}{\eta}\left(\frac{r_{2i}}{G_2 J_2} + \frac{r_{1o}}{G_1 J_1}\right)\tau_{2i} - \frac{2\pi a^2 G_a \tau_{2iL} r_{1o}}{\eta G_1 J_1}. \tag{49}$$

Equation (49) is a second-order ordinary differential equation which can be rewritten in the following form

$$\frac{d^2\tau_{2i}}{dz^2} = a^2\tau_{2i} - \delta\tau_{2iL} \tag{50}$$

where, δ, ϕ, α were already defined by Eqs. (33), (34) and (35). The boundary conditions for Eq. (50) are:

$$\text{at } z = 0, \quad \tau_{2i} = 0 \tag{51}$$

$$\text{at } z = L, \quad \tau_{2i} = \tau_{2iL} = \frac{Tr_{2i}}{J_2} \tag{52}$$

The solution for the adherend stress, τ_{2i}, is:

$$\tau_{2i} = \frac{Tr_{2i}}{J_2}\left[\phi(1 - \cosh(\alpha z)) + \left(\frac{1 - \phi(1 - \cosh(\alpha L))}{\sinh(\alpha L)}\right)\sinh(\alpha z)\right] \tag{53}$$

From Eq. (8), the adhesive shear stress is given by

$$\tau_a = \frac{T\alpha}{2\pi a^2}\left[\left(\frac{1 - \varphi(1 - \cosh(\alpha L))}{\sinh(\alpha L)}\right)\cosh(\alpha z) - \varphi\cdot\sinh(\alpha z)\right] \tag{54}$$